Density Functional Studies of the Formation of Nitrous Acid from the Reaction of Nitrogen Dioxide and Water Vapor

Arthur Chou, Zhiru Li,† and Fu-Ming Tao*

Department of Chemistry and Biochemistry, California State University at Fullerton, Fullerton, California 92834

Received: February 8, 1999; In Final Form: July 12, 1999

Reaction mechanisms for the production of nitrous acid (HONO) from the homogeneous gas-phase hydrolysis of nitrogen dioxide (NO_2) are examined by density functional theory calculations. The molecular structures and energies of the $NO_2-(H_2O)_n$ ($n = 1, 2, 3$) and $N_2O_4-(H_2O)_n$ ($n = 1, 2$) systems corresponding to the stationary points on the potential energy surface along the reaction pathways are calculated using the B3LYP method with the 6-311+G(2d,p) basis set. These reaction pathways represent the homogeneous hydrolysis of NO_2 or N_2O_4 with a varying number of water (H_2O) molecules. The reactions of NO_2 with water produce HONO, along with the OH radical which was postulated to combine in the next step with a second NO_2 to form nitric acid (HNO_3). The simple $NO_2 + H_2O$ bimolecular reaction leads to the highly unstable OH radical which reacts reversibly with HONO without an energy barrier. The introduction of single solvating H_2O molecule appears to stabilize the transition state as well as an intermediate that contains the OH radical. However, the energy barrier is found to be near 30 kcal mol^{-1} and is not affected by multiple additional H_2O molecules. On the other hand, the reaction of N_2O_4 with water leads directly to HONO and HNO_3. The energy barrier for the N_2O_4 reaction is above 30 kcal mol^{-1} and is also unaffected by additional H_2O molecules. The study demonstrates that the gas-phase hydrolysis of NO_2 or N_2O_4 is insignificant regardless of water vapor pressure. The physical origin responsible for the unusual hydrolysis reaction of NO_2 is explored with the contrasting examples of N_2O_5 and SO_3 hydrolysis reactions.

I. Introduction

Nitrous acid (HONO) has long been recognized as an important trace gas in the tropospere where its rapid photolysis represents a significant source of hydroxy (OH) radicals. During the night, HONO has been observed to accumulate to concentrations up to 15 ppb, and this accumulation of HONO has a profound impact on the daytime chemistry of the troposphere. A computer simulation study showed that the photolysis of HONO accumulated over nighttime contributed to a 5-fold increase in the concentration of OH radicals in the early morning, and a 14% overall increase by noon.[1] The sources of HONO, particularly at night, are not well understood despite its well recognized importance. The literature has so far discussed three major sources of HONO. First, HONO was measured to be directly emitted through primary emission. However, studies have shown that this source does not contribute significantly to the nighttime concentration of HONO.[2] A second source of HONO is the reaction of NO with OH radicals. This reaction is also unlikely to contribute significantly to nighttime HONO formation as OH concentration is very low during the night.[3] A third source of HONO is the hydrolysis of nitrogen oxides (NO_x) in water vapor, which has been widely discussed in the literature. Two major reactions have been studied for the hydrolysis of NO_2:

$$2NO_2 + H_2O \rightarrow HONO + HNO_3 \quad (1)$$

$$NO + NO_2 + H_2O \rightarrow 2HONO \quad (2)$$

Numerous studies have shown reaction 2 to be less significant, as HONO has been produced in smog chambers without the presence of NO, and the rate of HONO production was independent of NO concentration.[1,4,5] Finally, NO_2 was found to be rapidly reduced to HONO on soot, presumably by a reactive site on the soot particle surface.[6−8]

NO_2 has long been known to react with water vapor to produce HONO as shown in reaction 1. The mechanism of this reaction has been the subject of many studies.[1,4,5,9,10] All of these studies show that the reaction of NO_2 with water vapor is more complex than its simple stoichiometry suggests. By measuring the HONO formation rates at different initial NO_2 and H_2O concentrations, these studies established that the reaction is approximately first order with respect to both [NO_2] and [H_2O].[1,4,5] This suggests that reaction 1 is not an elementary termolecular reaction. In addition, the reaction rate was also found to be influenced by the material of the reaction chamber surface and the surface to volume ratio.[4,5]

Such findings have led to numerous proposals of the surface-catalyzed reaction mechanism for reaction 1. Pitts and coworkers[5] proposed three possible mechanisms involving the reaction of adsorbed species. In two of the mechanisms the first and rate determining step was the adsorption of NO_2 on the wall, while in the third mechanism the first and rate determining step was the formation of the $NO_2 \cdot H_2O$ complex on the wall.[5] Subsequent studies suggested that the first two mechanisms were unlikely because the formation of HONO was too slow to be diffusion controlled.[1] The third mechanism, also supported by Jenkins and co-workers,[1] has the following two steps,

$$NO_2(ads) + H_2O(ads) \rightarrow NO_2 \cdot H_2O(ads) \quad (3)$$

* Author to whom correspondence should be addressed.
† On leave from Department of Chemistry, Jilin University, Changhun, China.

10.1021/jp990465f CCC: $18.00
Published on Web 09/08/1999

$$NO_2(ads) + NO_2{\cdot}H_2O(ads) \rightarrow HNO_3(ads) + HONO(g) \quad (4)$$

Such a mechanism successfully accounts for the first order dependence on NO_2 concentration, with the condition that reaction 3 is the rate-determining step.[9]

The homogeneous gas-phase reaction of NO_2 with H_2O was considered to be insignificant, as the derived rate constant was too small to account for HONO formation.[11] Field studies showed that the rate of HONO formation was influenced by aerosol parameters, as the rate of nitrous acid formation was correlated with total aerosol surface areas.[12,13] It is conceivable that a potentially significant reaction pathway could be a gas-phase reaction catalyzed by aerosol particles or particulate water molecules. Such a mechanism was indeed hypothesized to exist.[3,12,13] It has been shown that although the reaction of NO_2 with bulk liquid water is very slow, the nature of the reaction of NO_2 with particulate water droplets remains unclear and may be an important source of HONO.[3]

The NO_2 molecules might also dimerize to form N_2O_4 before reacting with H_2O. However, isotope studies indicated that HONO formation in the gas phase was unlikely to involve N_2O_4 at room temperature range.[4] This observation is supported by the first order dependence of the reaction rate on NO_2 concentration.

Many other observations are still left unexplained. First, in both field and smog chamber studies, the HONO formed was found to plateau after a period of time, implying that HONO was being removed or that HONO formation was an equilibrium reaction.[1,3] Second, nitric oxide (NO) and OH radicals were found to be produced in smog chambers whose sources were unclear.[1,4,5,14,15] Finally, the reaction rate was found to have a negative temperature dependence.[1,9] As a result, it seems that an exclusive surface reaction mechanism cannot satisfactorily explain all these experimental observations.

In this paper, we present results of a theoretical investigation onthe reaction of nitrogen dioxide and water to form nitrous acid using the density functional theory (DFT). We attempt to answer whether or not the homogeneous gas-phase hydrolysis of nitrogen dioxide is possible at all without the involvement of any other species except water. Our more specific plan is to study reaction 1 with an emphasis on the effect of additional water molecules on the reaction through several proposed pathways of reaction 1 that involve a different number of water molecules and also N_2O_4, the dimer of NO_2. The stationary points on the reaction pathways are characterized by DFT calculations.Discussions based on the calculated results are given to understand some of the experimental observations, particularly the effect of water vapor on the hydrolysis of NO_2. Although only gas-phase reactions are explicitly considered, implications of our results on heterogeneous reactions are also discussed. Finally, comparisons with the hydrolysis of other oxides, such as dinitrogen pentoxide (N_2O_5) and sulfur oxide (SO_3), are given to understand the hydrolysis of NO_2.

II. Methods of Calculation

Five different pathways of reaction 1 are considered, each of which involves the NO_2 monomer or the dimer (N_2O_4) with a varying number (n) of water molecules. For the NO_2 reactions, the number of water molecules varies from one, two, to three, and the corresponding reaction paths are denotedpathways I, II, and III, respectively. These pathways are assumed to proceed in the general schematic steps as follows,

Step 1: $NO_2 + nH_2O \rightarrow NO_2{\cdot}(H_2O)_n$, ($n = 1$, 2, or 3)

Step 2: $NO_2{\cdot}(H_2O)_n \rightarrow HONO{\cdot}OH{\cdot}(H_2O)_{n-1}$

Step 3: $HONO{\cdot}OH{\cdot}(H_2O)_{n-1} + NO_2 \rightarrow HONO{\cdot}HNO_3{\cdot}(H_2O)_{n-1}$

Step 4: $HONO{\cdot}HNO_3{\cdot}(H_2O)_{n-1} \rightarrow HONO + HNO_3 + (n-1)H_2O$

In step 1, the reactant species ($NO_2 + nH_2O$) form the reactant complex $NO_2{\cdot}(H_2O)_n$. The resulting complex then reacts in the next step, passing through the transition state (TS) and forming a reaction intermediate $HONO{\cdot}OH{\cdot}(H_2O)_{n-1}$ that contains HONO and OH fragments. In step 3, the reaction intermediate reacts with a second NO_2 molecule to form the product complex $HONO{\cdot}HNO_3{\cdot}(H_2O)_{n-1}$. Finally in step 4, the product complex dissociates into separate product molecules. The net reaction is reaction 1 and is identical for all of the three pathways.

For the dimer (N_2O_4) reactions, the number of water molecules involved varies from one to two, and the corresponding pathways are denoted pathways IV and V, respectively. Similar to the NO_2 reactions, the N_2O_4 reactions are assumed to proceed in the following schematic steps,

Step 1: $N_2O_4 + nH_2O \rightarrow N_2O_4{\cdot}(H_2O)_n$, ($n = 1$ or 2)

Step 2: $N_2O_4{\cdot}(H_2O)_n \rightarrow HONO{\cdot}HNO_3{\cdot}(H_2O)_{n-1}$

Step 3: $HONO{\cdot}HNO_3{\cdot}(H_2O)_{n-1} \rightarrow HONO + HNO_3 + (n-1)H_2O$

The first and third steps are, respectively, the formation of the reactant complex and the dissociation of the product complex. The second step transforms the reactant complex to the product complex, passing through a transition state. In contrast with the NO_2 monomer reactions, the dimerreactions involve no reaction intermediate. The overall reaction is $N_2O_4 + H_2O \rightarrow HONO + HNO_3$.

The molecular species identified in the above reaction steps correspond to the stationary points on the potential energy surface along the reaction pathway considered. Equilibrium geometries of these species, including those of the transition states as well as the separate reactant and product molecules, are calculated using density functional theory. The three-parameter hybrid method of Becke[16−18] with the local and nonlocal functionals of Lee, Yang, and Parr [19] (B3LYP) is efficient and reliable for studying chemical reactions[20] and hydrogen-bonded systems,[21,22] and is employed as the primary method of our calculations. Two different basis sets, 6-31G*[23,24] and 6-311+G(2d,p),[25] were used in the search for the equilibrium geometries. The resulting geometries are essentially the same, and so only those of the larger basis set are reported here. The harmonic frequencies were calculated using the B3LYP method with the 6-311+G(2d,p) basis set. The energy of reaction and the energy barrier for reaction II were also calculated with several other basis sets to examine the convergence with basis set. Zero-point vibrational energy is considered on the basis of calculated harmonic frequencies.

Transition structures were located using the synchronous transit quasi-Newton method[26,27] and were verified by subsequent frequency calculations and by intrinsic reaction coordinate (IRC) calculations.[28] All calculations were performed using the GAUSSIAN 94 program.[29]

TABLE 1: Calculated and Experimental Geometries, Dipole Moments, and Harmonic Frequencies of the Reactants and Products for the Reaction Pathways I−V[a]

molecule	geometry			dipole		harmonic frequecies		
(symmetry)	parameter	calcd	exptl	calcd	expt	mode	calcd	exptl
H_2O	r(OH)	0.963	0.958	2.082	1.854	*s*-str	3811	3832[b]
(C_{2v})	∠HOH	105.2	104.5			*a*-str	3915	3943
						bend	1618	1648
NO_2	r(NO)	1.194	1.193	0.348	0.316	*s*-str	1381	1318
(C_{2v})	∠ONO	134.3	134.1			*a*-str	1672	1618
						bend	761	750
OH	r(OH)	0.977	0.977[c]	1.777	1.668[c]	str	3700	3735
N_2O_4	r(NN)	1.793	1.782	0.000	0.000	NO_2 *s*-str	1437	1382[d]
(D_{2h})	r(NO)	1.188	1.190			NO_2 *s*-bend	843	812
	∠ONO	134.7	135.4			N-N str	295	281
						torsion	85	79
						NO_2 *a*-str	1765	1724
						NO_2 *a*-rock	498	498
						NO_2 *s*-wag	442	436
						NO_2 *a*-wag	704	677
						NO_2 *a*-str	1799	1757
						NO_2 *s*-rock	228	265
						NO_2 *s*-str	1299	1261
						NO_2 *a*-bend	759	751
HONO	r(NO_H)	1.433	1.432	2.062	1.854	OH str	3757	3591[e]
(trans, C_s)	r(NO)	1.165	1.170			N═Ostr	1764	1700
	r(OH)	0.980	0.958			HON bend	1301	1263
	∠HON	102.7	102.1			N−O str	817	790
	∠ONO	110.7	111.1			ONO bend	617	596
						torsion	580	544
HONO	r(NO_H)	1.392	1.39	1.577	1.423	OH str	3588	3426[e]
(cis, C_s)	r(NO)	1.179	1.19			N═Ostr	1697	1641
	r(OH)	0.980	0.98			HON bend	1339	1302
	∠HON	106.2	104.			N−O str	875	852
	∠ONO	113.8	114.			ONO bend	689	609
						torsion	631	640
HNO_3	r(NO_H)	1.411	1.41	2.363	2.17	OH str	3725	3550[f]
(C_s)	r(OH)	0.973	0.960			NO_2 *a*-str	1738	1709[f]
	r(NO_{cis})	1.195	1.21			NO_2 *s*-str	1345	1326[g]
	r(NO_{trans})	1.211	1.20			NOH bend	1320	1304[g]
	∠HON	103.2	102.2			NO_H str	904	878[f]
	∠ONO_{trans}	115.7	115.9			NO_2 bend	652	647[h]
	∠ONO_{cis}	114.0	113.9			ONO_H bend	586	580[h]
						NO_2 wag	783	763[h]
						ONOH torsion	473	458[i]

[a] Experimental values, if not indicated, are from ref 30. [b] Reference 31. [c] Reference 32. [d] Reference 33. [e] Reference 34. [f] Reference 35. [g] Reference 36. [h] Reference 37. [i] Reference 38. [j] Str = stretch. wag = wagging.

III. Results of Calculation

The results of calculation are summarized in Tables 1 and 2 and Figure 1. Table 1 presents the equilibrium geometries, dipole moments, and harmonic frequencies of the reactant and product molecules from B3LYP/6-311+G(2d,p) calculations along with the available experimental comparisons [30−38]. Figure 1 shows the optimized geometries of the complexes of reactants, products, and the transition state involved in reactions I to V. Table 2 presents calculated total energies, zero-point vibrational energies (ZPVE) and dipole moments of all the species considered. Table 3 shows the basis set dependence of the total energies and relative energies for reaction II. Table 4 presents the relative energies of the species for reactions I to V without and with ZPVE corrections.

It is clear from Table 1 that our calculated molecular properties for the reactants and products are in very good agreement with experiment. Almost all of the calculated bond lengths and bond angles are, respectively, within 0.01 Å and 1° from the experimental values. The calculated dipoles are consistently 10% larger than the experimental values, which is typical of the DFT method. The calculated harmonic frequencies are mostly within 2% of experimental values. The level of agreement of the calculated properties with experiment is generally better than would be expected for calculations using Hartree−Fock or MP2 (second-order Møller−Plesset approximation) method.

The calculated relative energies from several basis sets shown in Table 3 indicate that the calculated energetics are adequately converged with respect to the increase of basis set size. Specifically, the energy barrier ($E^{\neq}$) increases quickly from 16.1 kcal mol^{-1} to 25.0 kcal mol^{-1} as the basis set used changes from 6-31G(d) to 6-311+G(2d,p) and stabilizes to 26.2 kcal mol^{-1} as the basis set further changes to 6-311++G(2d,2p). Similarly, the energy of reaction (ΔE) changes drastically from 12.8 kcal mol^{-1} to 7.9 kcal mol^{-1} as the basis set changes from 6-31G(d) to 6-311+G(2d,p) but stays almost constant (7.8 kcal mol^{-1}) with the 6-311++G(2d,2p) basis set. It should be noted that, although the values of $E^{\neq}$ and ΔE from the 6-31G(d) basis set are not converged, the geometries are well converged, as shown by the energy calculation with the 6-311+G(2d,p) basis set using the 6-31G(d) geometries.

A. Pathway I: $NO_2 + H_2O \rightarrow HONO + OH \xrightarrow{NO_2} HONO + HNO_3$. As the NO_2 molecule is approached by the H_2O molecule, the system first reaches a potential minimum corresponding to the weakly bounded complex, $NO_2 \cdot H_2O$. Two

TABLE 2: Total Energies (hartrees), Zero-Point Vibrational Energies (ZPVE, kcal mol^{-1}), and Dipole Moments (D) of the Various Species Involved in the Reaction Pathways I−V from B3LYP Calculations with the 6-311+G(2d,p) Basis Set

molecule	total energy	ZPVE	dipole
H_2O	−76.459 526	13.36	2.082
NO_2	−205.145 964	5.45	0.348
HONO (trans)	−205.776 678	12.63	2.062
HONO (cis)	−205.776 052	12.61	1.576
HNO_3	−280.987 349	16.48	2.363
OH	−75.763 164	5.29	1.777
$(H_2O)_2$	−152.927 762	28.98	2.838
$(H_2O)_3$	−229.404 842	45.78	1.145
$NO_2{\cdot}H_2O$ (a)	−281.606 921	19.21	2.626
$NO_2{\cdot}H_2O$ (b)	−281.606 971	19.56	2.278
$NO_2{\cdot}(H_2O)_2$	−358.078 280	35.68	1.824
$NO_2{\cdot}(H_2O)_3$	−434.552 136	51.69	1.973
N_2O_4	−410.313 744	14.52	0.000
$N_2O_4{\cdot}H_2O$(a)	−486.780 059	29.03	2.403
$N_2O_4{\cdot}H_2O$(b)	−486.775 163	28.72	2.281
$N_2O_4{\cdot}(H_2O)_2$	−563.251 100	44.83	1.561
TS2($NO_2{\cdot}(H_2O)_2$)	−358.025 161	34.08	2.434
TS3($NO_2{\cdot}(H_2O)_3$)	−434.498 530	49.60	4.013
TS4($N_2O_4{\cdot}H_2O$)	−486.721 347	27.44	3.087
TS5($N_2O_4{\cdot}(H_2O)_2$)	−563.190 945	42.61	3.643
$HONO{\cdot}OH{\cdot}H_2O$	−358.029 060	36.49	2.030
$HONO{\cdot}OH{\cdot}(H_2O)_2$	−434.506 675	53.63	3.413
$HONO{\cdot}HNO_3$	−486.768 962	29.00	2.043
$HONO{\cdot}HNO_3{\cdot}H_2O$	−563.247 374	45.87	3.075
$HONO{\cdot}HNO_3{\cdot}(H_2O)_2$	−639.721 077	61.68	2.636

minimum geometries, shown in Figure 1, are found for the complex with nearly the same well depth $D_e = 0.9$ kcal mol^{-1}. $NO_2{\cdot}H_2O$ (a) has a C_{2v} symmetry with the O atom of H_2O pointing at the N atom of NO_2. $NO_2{\cdot}H_2O$ (b) contains a hydrogen bond between H_2O and NO_2. As the two molecules get closer, an H atom of H_2O starts to break away and approach toward the O atom of NO_2. The energy of the system increases drastically, leading to the formation of energetically less stable HONO and OH species. The sum of the separate HONO and OH energies is 41.2 kcal mol^{-1} above the sum of the separate NO_2 and H_2O energies, and no energy barrier is found for the reverse reaction of HONO and OH. Apparently, the bimolecular reaction of NO_2 and H_2O is highly unfavorable.

B. Pathway II: $NO_2 + 2\ H_2O \rightarrow HONO{\cdot}OH{\cdot}H_2O \xrightarrow{NO_2} HONO + HNO_3 + H_2O$. A second H_2O molecule is introduced to study its effect on the reaction of NO_2 and H_2O. Two possible roles are suspected to be played by the second H_2O in the reaction. It might actively participate in the reaction and act as a catalyst if a new H_2O molecule emerges in the final product. On the other hand, the H_2O might remain as an inert molecule throughout the reaction and therefore behave just as a solvent molecule in liquid water or a substrate molecule on a solid surface.

The three molecules first reach a potential minimum corresponding to the intermolecular complex $NO_2{\cdot}(H_2O)_2$, with a well depth $D_e = 8.3$ kcal mol^{-1} and a geometry shown in Figure 1. The two H_2O molecules are positioned next to NO_2 to form a cyclic arrangement with two consecutive hydrogen bonds. Each of the H_2O molecules occupies approximately one of the two possible H_2O positions relative to NO_2 in the complexes $NO_2{\cdot}H_2O$(a) and $NO_2{\cdot}H_2O$(b). The hydrogen bond between the H_2O molecules is stronger than that between H_2O and NO_2, as shown by their bond distances. As the molecules are forced to get closer, the H atoms at both hydrogen bonds start to transfer from the donor O atoms to the corresponding acceptor O atoms. At the transition state, shown as TS(II) in Figure 1, an OH radical and an HONO emerge, along with a new H_2O molecule resulting from the initial H_2O losing an H atom to NO2 and gaining an H atom from the other H_2O. The H_2O connected by two hydrogen bonds in the $NO_2{\cdot}(H_2O)_2$ complex facilitates the exchange of an H atom in the reaction, giving away an H atom to NO_2, while accepting an H atom from the first H_2O. Beyond the transition state, the system reaches to a shallow potential minimum corresponding to a metastable intermediate, $HONO{\cdot}HO{\cdot}H_2O$. This intermediate then reacts with an additional NO_2 and form a product complex, $HONO{\cdot}HNO_3{\cdot}H_2O$, which dissociates into three product molecules: HONO, HNO_3, and H_2O. Clearly, the second H_2O participates in the reaction of NO_2 and H_2O and plays an active role as a catalyst.

The transition state has an energy of 25.0 kcal mol^{-1}, and the reaction intermediate has an energy of 22.6 kcal mol^{-1}, all relative to the sum of reactant energies. The activation energy for reaction II with ZPVE correction is 26.9 kcal mol^{-1}. With ZPVE correction, the reaction intermediate is equally stable as the transition state.

C. Pathway III: $NO_2 + 3\ H_2O \rightarrow HONO{\cdot}OH{\cdot}(H_2O)_2 \xrightarrow{NO_2} HONO + HNO3 + 2\ H_2O$. The three-water reaction of NO_2 is similar to the two-water reaction described above. As usual, the molecules first reach a potential minimum corresponding to the intermolecular complex $NO_2{\cdot}(H_2O)_3$ with a well depth $D_e = 17.3$ kcal mol^{-1} and a geometry shown in Figure 1. Compared to the complex $NO_2{\cdot}(H_2O)_2$, $NO_2{\cdot}(H_2O)_3$ has the third H_2O participating in the hydrogen bonding chain with other molecules. The hydrogen bonds appear to be stronger than those in the $NO_2{\cdot}(H_2O)_2$ complex, as shown by the shorter hydrogen bond distances and a larger gain in the well depth. As the reaction takes place, as represented by the approach of the H_2O next to the N atom of NO_2, an H atom departs from the H_2O and initiates the synchronous transfer of H atoms along the three hydrogen bonds to their acceptor O atoms. The net result is to pass an H atom from the approaching H_2O to the O atom of NO_2. The transition state, shown as TS(III) in Figure 1, appears to contain an OH radical, an HONO, and two H_2O molecules. The two additional H_2O molecules jointly facilitate the transfer of the H atom. Beyond the transition state, the system reaches a shallow potential minimum corresponding to a reaction intermediate, $HONO{\cdot}HO{\cdot}(H_2O)_2$. This reaction intermediate reacts with an additional NO_2 and form a product complex, $HONO{\cdot}HNO_3{\cdot}(H_2O)_2$, which dissociates into four product molecules: an HONO, an HNO_3, and two H_2O molecules.

The transition state has an energy of 16.3 kcal mol^{-1} and the reaction intermediate has an energy of 11.2 kcal mol^{-1}, all relative to the sum of reactant energies. With the corrections for zero-point vibrational energy, the activation energy for pathway III is 20.4 kcal mol^{-1}. With ZPVE correction, the reaction intermediate is 1.0 kcal mol^{-1} lower in energy than the transition state. It should be pointed out that the apparent decrease in the energy of the transition state or the intermediate from reaction II is a result of solvation energy of the added H_2O in reaction III. We will return to the effect of solvation energy in the next section. In summary, both of the additional H_2O molecules participate in the reaction of $NO_2 + H_2O$ to facilitate the transfer of an H atom.

D. Pathway IV: $N_2O_4 + H_2O \rightarrow HONO + HNO_3$. The N_2O_4 and H_2O molecules form an intermolecular complex, $N_2O_4{\cdot}H_2O$(a), with a potential minimum $D_e = 4.3$ kcal mol^{-1} and a geometry shown in Figure 1. A second potential minimum is found to correspond to a hydrogen-bonded geometry, $N_2O_4{\cdot}H_2O$ (b). However, the second geometry is much less stable because of the small well depth $D_e = 1.3$ kcal mol^{-1}. As the reaction takes place, the two NO_2 units of N_2O_4 start to

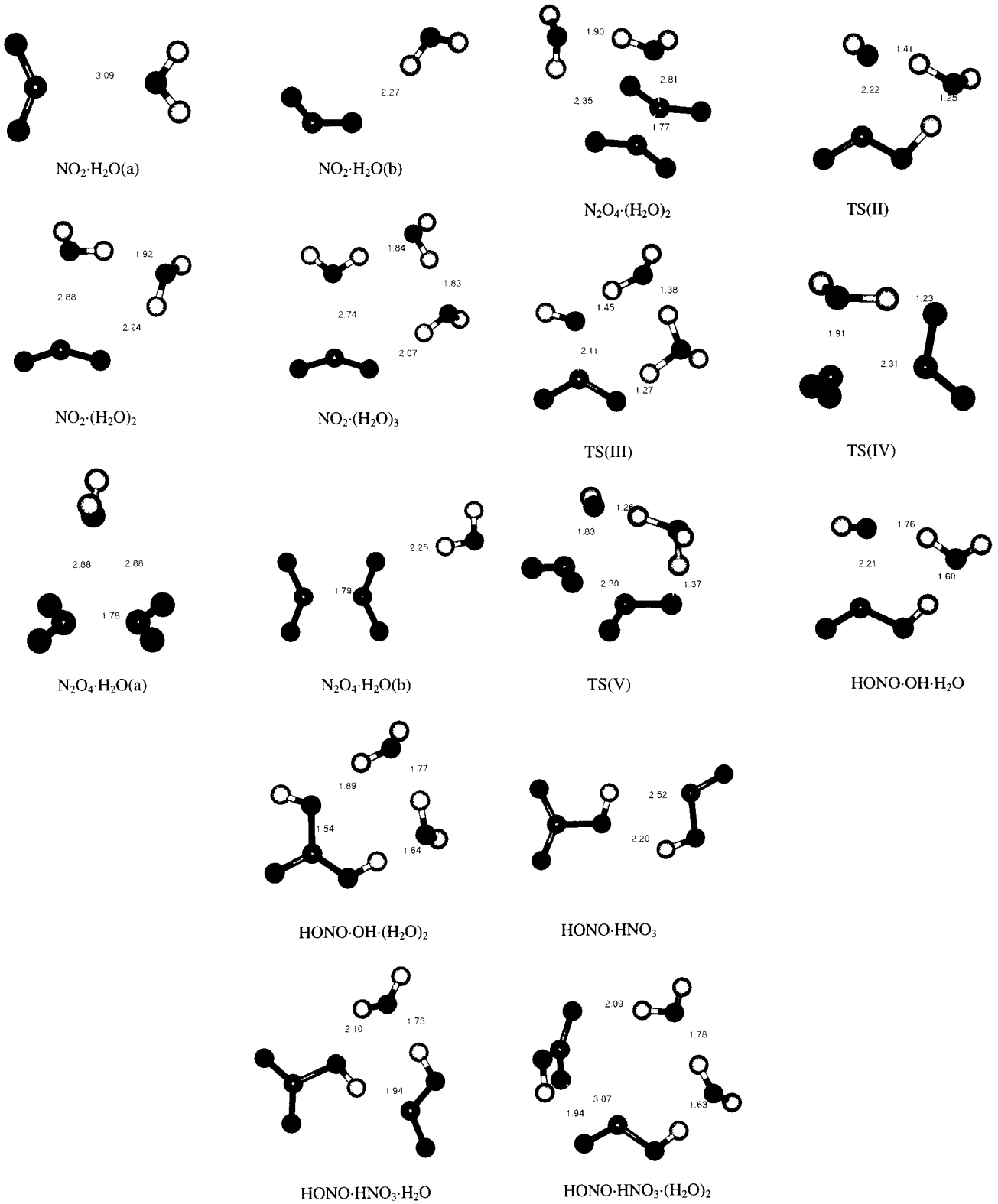

Figure 1. Equilibrium geometries corresponding to the stationary points on the reaction pathways I−V optimized at the level of B3LYP/6-311+G-(2d,p). Selected interatomic distances are given in angstroms.

depart from each other. The O atom of H_2O approaches an N atom of one NO_2 unit while an H atom of H_2O approaches an O atom of the other NO_2 unit. At the transition state, as shown as TS(IV) in Figure 1, the two NO_2 units match the H and OH fragments of H_2O, respectively, to form the HONO and HNO_3 product molecules.

The reaction has an energy barrier of 32.6 kcal mol^{-1} and a ZPVE-corrected activation energy of 32.1 kcal mol^{-1}. As a result, the reaction is not kinetically favorable. Moreover, the reaction is endothermic by 7.0 kcal mol^{-1}, and is not thermodynamically favorable.

E. Pathway V: $N_2O_4 + 2\,H_2O \rightarrow HONO + HNO_3 + H_2O$. The reactant molecules form an intermolecular complex, $N_2O_4 \cdot (H_2O)_2$, with a well depth of D_e = 11.5 kcal mol^{-1} and a geometry shown in Figure 1. The second H_2O is introduced to the system of N_2O_4 and H_2O to act as an acceptor of a strong

TABLE 3: Basis Set Dependence of the Total Energies (hartrees) and Relative Energies (kcal mol^{-1}) for the Species in Reaction Pathway II

basis set	$E_{reactants}$[a]	$E_{TS(II)}$	$E_{products}$[b]	$E^{\neq}$[c]	ΔE[d]
6−31G*/6−31G*	−562.962316	−562.936601	−562.982716	16.13	−12.80
6−311+G(2d,p)/6−31G*	−563.210240	−563.169961	−563.223259	25.28	−8.17
6−311+G(2d,p)	−563.210980	−563.171125	−563.223553	25.01	−7.89
6−311++G(2d,2p)	−563.215964	−563.174182	−563.228415	26.22	−7.81

[a] Equals to $2E(NO_2) + 2E(H_2O)$. [b] Equals to $E(HONO) + E(HNO_3) + E(H_2O)$. [c] Equals to $E_{TS(II)} - E_{reactants}$. [d] Equals to $E_{products} - E_{reactants}$.

TABLE 4: Relative Energies (kcal mol^{-1}) with Respect to the Separate Reactants for Reaction Pathways I−V

species	E	ZPVE	E + ZPVE
	Pathway I		
$NO_2 + H_2O$	0	0	0
$NO_2 \cdot H_2O$	−0.90	0.40	−0.50
HONO + OH	41.19	−0.89	40.30
HONO + HNO_3	−7.89	4.85	−3.04
	Pathway II		
NO_2+2H_2O	0	0	0
$NO_2 \cdot (H_2O)_2$	−8.32	3.51	−4.81
TS(II)	25.01	1.91	26.92
$HONO \cdot OH \cdot H_2O$	22.56	4.32	26.88
$HONO \cdot HNO_3 \cdot H_2O$	−22.84	8.24	−14.60
$HONO+HNO_3+H_2O$	−7.89	4.85	−3.04
	Pathway III		
NO_2+3H_2O	0	0	0
$NO_2 \cdot (H_2O)_3$	−17.32	6.15	−11.17
TS(III)	16.32	4.07	20.39
$HONO \cdot OH \cdot (H_2O)_2$	11.21	8.09	19.30
$HONO \cdot HNO_3 \cdot (H_2O)_2$	−31.73	10.69	−21.04
$HONO+HNO_3+2H_2O$	−7.89	4.85	−3.04
	Pathway IV		
$N_2O_4+H_2O$	0	0	0
$N_2O_4 \cdot H_2O$	−4.26	1.15	−3.11
TS(IV)	32.58	−0.44	32.14
$HONO \cdot HNO_3$	2.70	1.13	3.83
HONO + HNO_3	5.80	1.23	7.03
	Pathway V		
$N_2O_4 + 2H_2O$	0	0	0
$N_2O_4 \cdot (H_2O)_2$	−11.49	3.60	−7.89
TS(V)	26.26	1.37	27.63
$HONO \cdot HNO_3 \cdot H_2O$	−9.03	4.64	−4.39
HONO + HNO_3 + H_2O	5.80	1.23	7.03

hydrogen bond from the first H_2O, as well as a donor of a weak hydrogen bond to an O atom of N_2O_4. Similar to the reaction of N_2O_4 and H_2O, the N−N bond of N_2O_4 breaks apart to form two separate NO_2 units as the system of $N_2O_4 + 2\ H_2O$ reacts. The two H atoms at the hydrogen bonds transfer simultaneously from the donor to the acceptor atoms, analogous to the reaction of $NO_2 + 2\ H_2O$ described earlier. The O atom of H_2O closer to the N atom of one NO_2 unit approaches the N atom while an H atom of the second H_2O approaches an O atom of the other NO_2 unit. At the transition state, shown as TS(V) in Figure 1, the two NO_2 units match the H and OH fragments from the two H_2O molecule, to form the HONO and HNO_3 product molecules and a new H_2O molecule. Again, the second H_2O molecule plays an active role facilitating the transfer of an H atom, just as in the NO_2 reactions.

The reaction has an energy barrier of 26.3 kcal mol^{-1} and a ZPVE-corrected activation energy of 27.6 kcal mol^{-1}. Compared to the $N_2O_4 + H_2O$ reaction, the energy barrier is considerably lower but the lowering appears to be a result of solvation energy from the second H_2O. Compared to the $NO_2 + H_2O$ reaction, the energy barrier is slightly higher. The reaction is endothermic and is not thermodynamically favorable.

IV. Discussion

Our calculations have shown that all of the pathways (I−V) are characterized by high energy barriers, or large activation energies. This indicates that the homogeneous hydrolysis of NO_2 or N_2O_4 is unlikely to take place in typical atmospheric conditions, which is consistent with available experimental measusurements in smog-chamber and field studies.

TABLE 5: Activation Energies (kcal mol^{-1}) for Bimolecular Reactions of Various Clusters before Zero-Point Energy Correction (E_a) and after Zero-Point Energy Correction (E')$_a$

reactants	E_a	$(E')_a$
$NO_2 + H_2O$	∼41.19[a]	∼40.30[a]
$NO_2 + (H_2O)_2$	30.47	30.08
$NO_2 + (H_2O)_3$	32.75	31.09
$NO_2 \cdot H_2O + H_2O$	25.91	27.42
$NO_2 \cdot H_2O + (H_2O)_2$	22.68	24.05
$NO_2 \cdot (H_2O)_2 + H_2O$	24.64	25.20
$N_2O_4 + H_2O$	32.58	32.14
$N_2O_4 + (H_2O)_2$	31.72	30.79
$N_2O_4 \cdot H_2O + H_2O$	30.52	30.74

[a] No transition state was found. Activation energy was taken to be the energy required to form the isolated HONO and OH species.

It is important to point out that the energy values presented in Table 4 are relative to the sum of the energies of the isolated reactants involved in the reactions. The energy of the transition state, or the activation energy, appears to decrease with the increasing number of H_2O molecules involved in the reaction. However, such a decrease is largely attributed to the solvation energy of each added H_2O. The reactant complex and the transition state are both stabilized by the solvation energy of the added water. The more important quantity for showing the effect of water on the reaction should be the height of the energy barrier, or the relative energy of the transition state with respect to the reactant complex. This energy barrier is equivalent to the activation energy for the unimolecular reaction of the reactant complex. From the values in Table 4, one can see that the energy barrier does not change at all with the increase of water molecules involved. For instance, the (unimolecular reaction) activation energy is 31.7 kcal mol^{-1} for pathway II and is 31.6 kcal mol^{-1} for pathway III. Similar results can be seen for pathways IV and V. It is reasonable to expect that such a high energy barrier would not be appreciably lowered in larger water clusters. Clearly, the effect of additional water molecules on the hydrolysis of NO_2 is limited to providing the reacting system with a given amount of solvation energy that is nearly constant throughout the course of reaction.

The effect of water molecules may be more consistently shown if the reactions are all considered to start with a bimolecular elementary step that directly leads to the transition state. Table 5 lists the values of the activation energies for all the possible bimolecular reactions that involve the different total numbers of water molecules considered in this study. It is seen that the activation energy for the reaction of NO_2 with the water dimer is 30.1 kcal mol^{-1}, nearly identical to that for the reaction of NO_2 with the water trimer (31.1 kcal mol^{-1}). In other words, it appears that the activation energy for the reaction of NO_2 with a water cluster is nearly constant, regardless of the size of the cluster. This may explain the undetectable reaction of NO_2 with bulk liquid water.[3] The bimolecular reactions may also

include the reaction of a hydrated NO_2 and a water monomer or cluster. As shown in Table 5, the activation energy for the reaction of hydrated NO_2 appears to be about 5 kcal mol^{-1} lower than that for the reaction of NO_2 without hydration. This may suggest the surface catalyzed reaction of NO_2 with water can be aided by extra water. In this mechanism, the NO_2 molecules might first be absorbed on the surface, comparable to the state of being monohydrated or dihydrated, and then react with the approaching H_2O molecules fromthe gas phase. This mechanism was initially proposed by Pitts and co-workers[5] based on the results of chamber experiments.[4,5]

In contrast, the activation energy, 32.1 kcal mol^{-1}, for the reaction of the hydrated N_2O_4 with H_2O is not significantly lower than 31.7 kcal mol^{-1} for the reaction of the unhydrated N_2O_4 with H_2O. This may suggest that a surface catalyzed reaction similar to NO_2 is not valid for N_2O_4. As a result, the pathways involving the dimerization of NO_2 as the first step are even less favorable than those involving the direct hydrolysis of NO_2. N_2O_4 does not appear to be a significant source of atmospheric HONO, in agreement with the conclusions of Sakamaki et al.[4]

This study suggests that a homogeneous gas-phase mechanism for the hydrolysis of NO_2 is unlikely to account for the production of HONO in the natural atmosphere. However, it may still offer explanations to some intriguing smog-chamber and field observations. For example, it is possible that the hydrolysis of NO_2 can lead to the production of the OH radical as a reaction intermediate. An unknown continuous OH radical source was indeed observed in all of the chambers studied, which appeared to increase linearly with the NO_2 level and the H_2O vapor pressure.[1,4,5,14,15] The enhanced stability of the OH radical in the HONO·OH·H_2O complex might allow its reaction with HONO to form $NO_2 + H_2O$, the reverse of reaction 1. This may explain the declining NO_2 reaction rate with time and the concentration plateau of HONO observed in smog-chambers.[1] As more HONO is produced, the reaction of HONO + OH becomes more significant until eventually the rates of the forward and reverse reactions are equal and a dynamic equilibrum is reached. This hypothesis explains the observation that the HONO/NO_2 ratio stabilizies in the troposphere.[3]

The insignificant effect of multiple water molecules on the hydrolysis of NO_2 to form HONO is in stark contrast to the known effect of multiple water molecules on the hydrolysis reactions of dinitrogen pentoxide (N_2O_5) and sulfur trioxde (SO_3). The hydrolysis of N_2O_5 forms nitric acid (HNO_3) by the reaction $N_2O_5 + H_2O \rightarrow 2\ HNO_3$. The reaction was recently studied by theoretical calculations on the reaction pathways involving one, two, three, and four water molecules, respectively.[39,40] The energy barrier of each pathway, corresponding to the energy of the transition state relative to the reactant complex, was found to decrease progressively with the number of water molecules involved in the reaction. The barriers with one, two, and three water molecules are 24.3, 19.5, and10.4 kcal mol^{-1}, respectively. The energy barrier is completely eliminated with four water molecules, and the geometry optimization of $N_2O_5-(H_2O)_4$ leads directly to the product complex $(HNO_3)_2-(H_2O)_3$. These results are consistent with experimental observations that the homogeneous gas-phase hydrolysis of N_2O_5 is too slow to be noticeable[41] but that the hydrolysis in bulk water can be completed instantaneously.[42] Very similar results were found for the hydrolysis of SO_3 to form sulfuric acid (H_2SO_4).[43−45] Most significantly, the energy barrier for the reaction of SO_3 with four water molecules was also found to completely disappear.[45]

One might wonder why the hydrolysis of NO_2 appears to have such strikingly different energetics from the hydrolysis of N_2O_5 and SO_3. Here we offer a possible answer to such a question. The origin of the difference may lie in the physical state of the transition state in each reaction. The hydrolysis of N_2O_5 is initiated by the nucleophilic attack on N_2O_5 by water, resulting in a transition state that resembles the ion pair $H_2ONO_2^+ \cdot NO_3^-$.[39] Because of its ionic nature, the transition state is more favorably stabilized than the neutral reactant N_2O_5 by polar solvent such as water. In other words, the solvation energy by water increases, instead of being constant as in the case of NO_2, in going from the reactant to transition state. It is the disproportionally large solvation energy of the ionic transition state over the neutral reactant by water solvent that is largely responsible for the decreasing energy barrier with the increasing number of water molecules participating in the hydrolysis of N_2O_5. Very similarly, the hydrolysis of SO_3 results in a transition state that resembles the ion pair $H^+ \cdot HOSO_3^-$ and is more favorably stabilized than the neutral reactant SO_3 by water.[45] In contrast, the transition state for the hydrolysis of NO_2, as shown by the present study, contains an OH radical, rather than an ionic species as in the hydrolysis of N_2O_5 or SO_3. The solvation of OH radical by water solvent is not expected to be more favorable than the solvation of NO_2. As a result, the energy barrier for the hydrolysis of NO_2 is nearly constant with respect to addition of solvent water molecules.

V. Conclusion

Five reaction pathways for the production of nitrous acid (HONO) from the hydrolysis of nitrogen dioxide (NO_2) are examined by density-functional theory calculations using the B3LYP method with the 6-311+G(2d,p) basis set. These reaction pathways represent the homogeneous hydrolysis of NO_2 or N_2O_4 with a varying number of water (H_2O) molecules. The reaction of NO_2 with water produce HONO, along with the OH radical as a reaction intermediate which combines in the next step with a second NO_2 to form nitric acid (HNO_3). The simple $NO_2 + H_2O$ bimolecular reaction is impossible because it forms the highly unstable OH radical which reacts reversibly and spontaneously with HONO with no energy barrier. Additional H_2O molecules may be present to stabilize the transition state or the intermediate that contains the OH radical. However, the energy barrier, determined as the relative energy of the transition state with respect to the reactant complex with water, is unaffected by the presence of multiple water molecules and is too high to allow the reaction to be practically significant. A high energy barrier is also found for the reaction of N_2O_4 with water to directly produce HONO and HNO_3 and is unaffected by the presence of multiple water molecules. All the results indicate that the homogeneous gas-phase hydrolysis of NO_2 is not practically significant in the formation of HONO regardless of water vapor pressure, and that a heterogeneous process is most likely responsible. The results are also valuable for understanding some of the experimental observations. Final discussions are made to reveal and understand the physical origin responsible for the uniquely different and complicated hydrolysis reaction of NO_2, compared with the hydrolysis reactions of N_2O_5 and SO_3.

Acknowledgment. This work was supported by The American Chemical Society Petroleum Research Fund (ACS-PRF Grant 30399-GB6), The Research Corporation (Cottrell College Science Award), and The NSF Research Experience for Undergraduate (REU) Program at The Department of Chemistry

and Biochemistry, California State University, Fullerton. The authors thank Professor Barbara J. Finlayson-Pitts and Professor John Olmsted, III, for helpful discussions.

References and Notes

(1) Jenkins, M. E.; Cox, R. A.; Williams, D. J. *Atmos. Environ.* **1988**, *22*, 487.
(2) Kirchstetter, T. W.; Harley, R. A.; Littlejohn, D. *Environ. Sci. Technol.* **1996**, *30*, 2843.
(3) Lammel, G.; Cape, J. N. *Chem. Soc. Rev.* **1996**, *25*, 361.
(4) Sakamaki, F.; Hatakeyama, S.; Akimoto, H. *Int. J. Chem. Kinet.* **1983**, *15*, 1013.
(5) Pitts, J. N.; Sanhueza, E.; Atkinson, R.; Carter, W. P. L.; Winer, A. M.; Harris, G. W.; Plum, C. N. *Int. J. Chem. Kinet.* **1984**, *19*, 919.
(6) Ammann, M.; Kalberer, M.; Jost, D. T.; Tobler, L.; Rossler, E.; Piguet, D.; Gaggeler, H. W.; Baltensperger, U. *Nature* **1998**, *395*, 157.
(7) Kalberer, M.; Ammann, M.; Arens, F.; Gaggeler, H. W.; Baltensperger, U. *J. Geophys. Res.* **1999**, *104*, 13825.
(8) Longfellow, C. A.; Ravishankara, A. R.; Hanson, D. R. *J. Geophys. Res.* **1999**, *104*, 13833.
(9) Svensson, R.; Ljungstrom, E.; Lindqvist, O. *Atmos. Environ.* **1987**, *21*, 1529.
(10) Lammel, G.; Perner, D.; Warneck, P. *Physico-Chemical Behaviour of Atmospheric Pollutants*; Proceedings of the 5th European Symposium, Varese, Italy, Sept. 25−28, 1989; Restelli, G., Angeletti, G., Eds.; pp 469−476.
(11) Kaiser E. W.; Wu, C. H. *J. Phys. Chem.* **1977**, *81*, 1701.
(12) Notholt, J.; Hjorth, J.; Raes, F. *Atmos. Environ.* **1992**, *26A* 211.
(13) Andres-Hernandez, M. D.; Notholt, J.; Hjorth, J.;Schrems, O. *Atmos. Environ.* **1996**, *30*, 175.
(14) Carter, W. P. L.; Atkinson, R.; Winer, A. M.; Pitts, J. N. *Int. J. Chem. Kinet.* **1982**, *14*, 1071.
(15) Lammel, G. *Atmos. Environ.* **1996**, *30*, 4101.
(16) Becke, A. D. *J. Chem. Phys.* **1992**, *96*, 2155.
(17) Becke, A. D. *J. Chem. Phys.* **1992**, *97*, 9173.
(18) Becke, A. D. *J. Chem. Phys.* **1993**, *98*, 5648.
(19) Lee, C.; Yang, W.; Parr, R. G. *Phys. Rev. B* **1988**, *37*, 785.
(20) Diau, E. W.-G.; Smith, S. C. *J. Chem. Phys.* **1997**, *106*, 9236.
(21) Kim, K.; Jordan, K. D. *J. Phys. Chem.* **1994**, *98*, 10089.
(22) Rablen, P. R.; Lockman, J. W.; Jorgensen, W. L. *J. Phys. Chem. A* **1998**, *102*, 3782.
(23) Ditchfield, R.; Hehre, W. J.; Pople, J. A. *J. Chem. Phys.* **1971**, *54*, 724.
(24) Hehre, W. J.; Ditchfield, R.; Pople, J. A. *J. Chem. Phys.* **1972**, *56*, 2257.
(25) Krishnan, R.; Binkley, J.; Seeger, R.; Pople, J. A. *J. Chem. Phys.* **1980**, *72*, 650.
(26) Peng, C.; Ayala, P. Y.; Schlegel, H. B.; Frisch, M. J. J. *Comput. Chem.* **1996**, *17*, 49.
(27) Peng, C.; Schlegel, H. B. *Isr. J. Chem.* **1994**, *33*, 449.
(28) Gonzalez, C.; Schlegel, H. B. *J. Phys. Chem.* **1989**, *90*, 2154.
(29) Frisch, M. J.; Trucks, G. W.; Schlegel, H. B.; Gill, P. M. W.; Johnson, B. G.; Robb, M. A.; Cheeseman, J. R.; Keith, T.; Petersson, G. A.; Montgomery, J. A.; Raghavachari, K. Al-Laham, M. A.; Zakrzewski, V. G.; Ortiz, J. V.; Foresman, J. B. Cioslowski, J.; Stefanov, B. B.; Nanayakkara, A.; Challacombe, M.; Peng, C. Y.; Ayala, P. Y.; Chen, W.; Wong, M. W.; Andres, J. L. Replogle, E. S.; Gomperts, R.; Martin, R. L.; Fox, D. J. Binkley, J. S.; Defrees, D. J.; Baker, J.; Stewart, J. P. Head-Gordon, M.; Gonzalez, C. and Pople, J. A. *Gaussian 94*, Revision D.2; Gaussian, Inc., Pittsburgh, PA, 1995.
(30) Lide, D. R. *CRC Handbook of Chemistry and Physics*; CRC Press: Boca Raton, 1996.
(31) Strey, G. *J. Mol. Spectrosc.* **1967**, *24*, 87.
(32) Townes, C. H.; Schawlow, A. L. *Microwave Spectroscopy*; Dover Publications, Inc.: New York, 1975.
(33) Melen, F.; Pokorni, F.; Herman, M. *Chem. Phys. Lett.* **1992**, *194*, 181.
(34) Murto, J.; Rasanen, M.; Aspiala, A.; Lotta, T. *J. Mol. Struct.* **1985**, *122*, 289.
(35) McGraw, G. E.; Bernitt, D. L.; Hisatsune, I. C. *J. Chem. Phys.* **1965**, *42*, 237.
(36) Perrin, A.; Lado-Bordowsky, O.; Valentini, A. *Mol. Phys.* **1989**, *67*, 249.
(37) Goldman, A.; Burkholder, J. B.; Howard, C. J.; Escribano, R.; Maki, A. G. *J. Mol. Spectrosc.* **1988**, *131*, 195.
(38) Maki, A. G.; Olson, W. B. *J. Mol. Spectrosc.* **1989**, *133*, 171.
(39) Hanway, D.; Tao, F.-M. *Chem. Phys. Lett.* **1998**, *285*, 459.
(40) Snyder, J. A.; Mendez, J.; Hanway, D.; Tao, F.-M. To be published.
(41) Wincel, H.; Mereland, E.; Castleman, A. W., Jr. *J. Phys. Chem.* **1994**, *98*, 8606.
(42) Hanson, D. R. *Geophys. Res. Lett.* **1997**, *24*, 1087.
(43) Kolb, C. E.; Jayne, J. T.; Worsnop, D. R.; Molina, M. J.; Meads, R. F.; Viggiano, A. A. *J. Am. Chem. Soc.* **1994**, *116*, 10314.
(44) Morokuma, K.; Muguruma, C. *J. Am. Chem. Soc.* **1994**, *116*, 10316.
(45) Larson, L. J.; Kuno, M.; Tao, F.-M. To be published.